Chapter 2
Literature Review

2.1 An Overview of Aerodynamic Entrainment of Dust Particles into Air

Aerodynamic forces acting on a dust layer can dislodge particles or clumps of particles from the layer and set them into motion. The entrainment of dust layers occurs in various modes or their combinations. Powders demonstrating negligible cohesion[1] tend to be removed as individual particles. More cohesive powders are removed as groups of particles (agglomerates), and sometimes, depending on layer and surface properties, appreciable portions of the layer can be lifted as a whole.

When the entire layer is subjected to uniform aerodynamic conditions (as in the case of pipe flow, or atmospheric flow) the dust may either be removed uniformly over the entire layer (erosion), or may be removed from the leading edge of the deposit. In this latter process called denudation, the leading edge of the deposit propagates in the direction of the flow. It is generally believed that for erosion type dust removal, adhesive forces must be larger than the cohesive forces.

As seen in Fig. 2.1, the particles removed from the layer can also show different types of behavior. Dislodged particles may roll on the surface until they find a spot with reduced fluid forces (such as a pit) and come to rest, or collide with another particle, thus transferring their momentum and aiding the removal of the new particle. During their travel, particles may even become airborne for short periods of time, yet still remain close to the surface. This type of transport is called surface creep. In another mode of transport called saltation, the particles are ejected from the surface almost vertically and are carried by the wind horizontally until they fall back onto the surface. Bagnold (1941) observed saltation layer thicknesses in the order of meters for desert sand. At higher air velocities, particles

[1] Conventionally, the word cohesion refers to the attraction force between two surfaces of the same material (such as the dust particles), whereas adhesion implies different materials (such as dust particle attracted to a plate)

E.A. Ural, *Towards Estimating Entrainment Fraction for Dust Layers*, SpringerBriefs in Fire, DOI 10.1007/978-1-4614-3372-9_2,

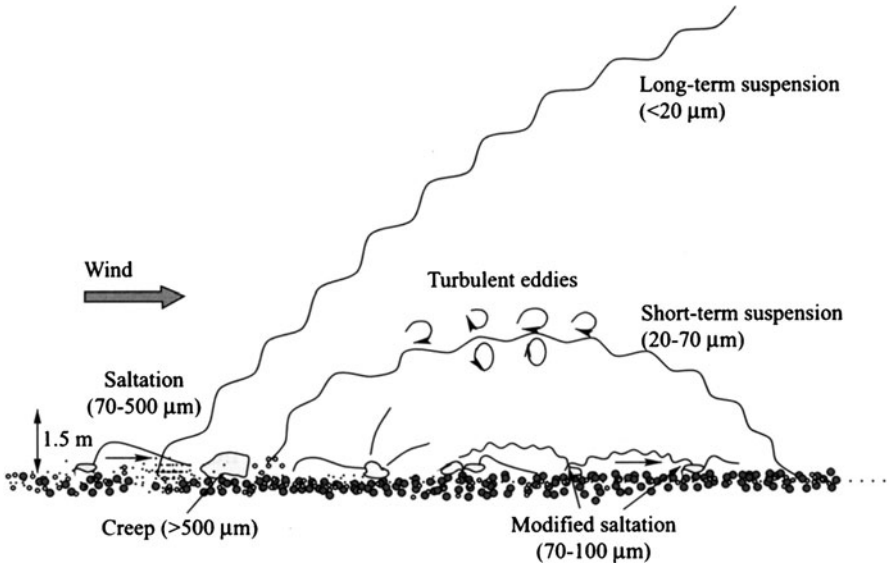

Fig. 2.1 Different types of sand particle motion that can occur during wind erosion (from Shao, 2008)

do not return to the surface (referred to as entering into suspension) and are carried for long distances.

Intuitively, it is easy to see whether a particle will be removed from a surface or from another particle, and the number of particles that get removed per unit time per unit surface area are governed by a balance between the forces trying to dislodge the particle, and the forces trying to keep the particle in place.

2.2 Characterization of the Aerodynamic Forces Acting on a Solid Particle

Extensive reviews of this subject are given by Clift (1978), and Yoshida et al (1979). Conventionally, aerodynamic force is resolved into two components: drag, in the direction of the mean flow; and lift, perpendicular to it. For uniform flow over a particle, the drag force is expressed by

$$F_D = CDA1/2\boldsymbol{\rho}U^2 \tag{2.1}$$

where C_D, A, $\boldsymbol{\rho}$, and U, respectively represent the particle drag coefficient, particle cross—sectional area, air density, and air velocity with respect to the particle.

At low relative velocities, the drag coefficient decreases with increasing Reynolds number. For spherical particles, an approximation to drag coefficient for Reynolds numbers smaller than 1000 is given by (Clift, 1978):

$$C_D = 24/Re\left(1 + 0.15Re^{2/3}\right) \tag{2.2}$$

where:

Re $\boldsymbol{\rho}$UD/μ particle Reynolds number;
D particle diameter;
μ viscosity of air.

The first term in this equation is called the Stokes drag coefficient, which constitutes the major portion of the drag for small particles. The corresponding Stokes drag can then be calculated as:

$$F_{Dst} = 3\pi\mu UD \tag{2.3}$$

A classical application of uniform flow over a sphere is the free fall of spheres. The terminal fall velocity is calculated by equating the drag force to the particle weight. In the Stokes regime (Re $<<$ 1) this is given by:

$$U_t = \rho_p g\ D2/(18\mu) \tag{2.4}$$

where ρ_p is the true density of the particle.

At high particle Reynolds numbers, the drag coefficient becomes independent of the Reynolds number so that the drag force is proportional to the square of both the relative velocity and the particle size, whereas the terminal velocity is proportional to the square root of the particle size and density.

The terminal velocity of an ensemble of monodisperse spherical particles in the absence of agglomeration is lower than that measured for an individual particle. This hindered settling problem has been studied in detail for monodisperse and polydisperse suspensions. Examples of such work can be found in Batchelor (1972), Batchelor and Wen (1982), and Davis and Birdsell (1988). The correction in the terminal velocity due to hindered settling is of the same order of magnitude as the volumetric fraction of the solid particles and should be negligible for most explosible dust clouds.

The drag force for low Reynolds number shear flow around a spherical particle is usually calculated by assuming the relative flow velocity as the undisturbed value at the particle center. This is rigorously accurate only for small particles exposed to constant velocity gradient because the Stokes drag force is proportional to the relative velocity. If the particle is adjacent to a wall, however, the drag force can be 70% higher than the Stokes drag, as suggested by the creeping flow solution of O'Neill (1968):

$$F_{Dw} = 8\mu\boldsymbol{\gamma}D^2 \tag{2.5}$$

where $\boldsymbol{\gamma}$ denotes the velocity gradient perpendicular to the wall. The effect of flow shear on particle drag is more difficult to assess at high Reynolds numbers due to flow separation phenomenon.

The lift force on a spherical particle is induced if the particle is rotating (axis of rotation perpendicular to the direction of flow) or is subjected to shear flow. Most work on this topic is concentrated on either very low or very high Reynolds numbers.

The lift force on a sphere spinning in a uniform flow was calculated for small Reynolds numbers by Rubinow and Keller (1961) as:

$$L = 1/8\pi\boldsymbol{\rho}D^3U\boldsymbol{\omega} \tag{2.6}$$

where $\boldsymbol{\omega}$ is the angular spin velocity. It is interesting to note that this solution is independent of viscosity, and is in a form similar to the Kutta—Joukowsky formula used to predict lift due to potential flow.

Saffman (1965) calculated a lift force exerted on a spherical particle by a shear flow. The formula he developed for low Reynolds numbers:

$$L = 1.61\boldsymbol{\rho\nu}^{1/2}\boldsymbol{\gamma}^{1/2}D^2U \tag{2.7}$$

where $\boldsymbol{\gamma}$ is the magnitude of the velocity gradient. Saffman's analysis has shown that up to the maximum spin attainable by free particles due to shear, the effect of angular velocity on the lift force is of higher order than the that calculated from the above equation. The velocity, U, in this equation is taken as the undisturbed velocity at the particle center. For a particle resting on a flat surface $U = \boldsymbol{\gamma}$ D/2, therefore:

$$Lw = 0.8\boldsymbol{\rho\nu}^{1/2}\boldsymbol{\gamma}^{3/2}D^3 \tag{2.8}$$

Another small Reynolds number particle lift mechanism was postulated by Cleaver and Yates (1973) for turbulent boundary layers. This model is based on the turbulent burst phenomenon occurring as sudden random eruptions in the boundary layer, transporting fluid near the wall towards the mean flow. Treating bursts as viscous stagnation flow, and somehow estimating the strength of the stagnation flow from the measurements of the mean velocity fluctuations normal to the wall, Cleaver and Yates (1973) proposed the following formula for particle lift due to turbulent burst:

$$L = 0.076\boldsymbol{\rho\nu}^{1/2}\boldsymbol{\gamma}^{3/2}D^3 \tag{2.9}$$

which is an order of magnitude smaller than the Saffman's lift.

The lift due to particle spin in uniform flow at high Reynolds numbers, called the Magnus force after its inventor, is well known to many tennis and golf players. The magnitude of this force is determined experimentally (see e.g., Clift (1978)), since the lift is generated by the formation of an asymmetric wake.

A sphere resting on a flat plate also experiences a lift force, as well as increased drag due to the presence of the wall, at high Reynolds numbers. Okamoto (1979) measured a lift coefficient $C_L = 0.242$, and drag coefficient $C_D = 0.627$ at $Re = 4.74 \times 10^4$.

The free stream turbulence is expected to have an important effect in the dispersion of a dust cloud once the particles are removed from the surface because it may control the extent of dispersion, settling rate and agglomeration/deagglomeration phenomena. A review of free stream turbulence effects on single particle behavior is given by Clift (1978). The particle dispersion by turbulence field is believed to be strongly dependent on the Stokes number, which is defined as the ratio of the characteristic particle response time to the time scale of the large scale eddies. The characteristic particle response time can be estimated as the ratio of terminal velocity to gravitational acceleration. At low Stokes numbers (i.e., particles with small settling velocity), the particles faithfully follow the fluid motion, and they are dispersed at approximately the fluid diffusion rate. At large Stokes numbers there is hardly any particle dispersion. Interestingly, there is an intermediate Stokes number regime in which particles may be dispersed faster than the fluid would, believed to be due to particles actually flinging out of eddies (e.g., Chein and Chung (1988)).

At intermediate—to—high Stokes numbers, mean particle drag may be decreased or increased due to presence of turbulence. Transition of flow around particle to turbulence is known to sharply reduce the drag coefficient. The presence of free stream turbulence causes this transition to occur at lower Reynolds numbers than critical. One of the mechanisms of increased particle drag is observed beyond the Stokes regime where the particle drag is a stronger than linear function of relative velocity. As a result of this functional dependence, a particle subjected to sinusoidal velocity fluctuations superposed on a mean flow should experience a larger increase in drag force during positive phase compared to the decrease in drag during the negative phase. When averaged over the cycle, therefore, a net increase in drag arises. As a result, a decrease in terminal velocity is observed in a fluctuating flow field. If the velocity fluctuations are of sufficient strength, the average terminal velocity reaches zero. The former phenomenon, called levitation, has been observed for solid particles suspended in liquid (Krantz et al (1973)).

In practically all scenarios of interest to this project, dust layers are formed over impermeable surfaces, and the disturbing air is forced to flow parallel to the solid boundary. The no-slip flow condition at the boundary inevitably imposes a boundary layer type flow phenomenon around the dust layer. Figure 2.2 shows a boundary layer velocity profile typical for turbulent flow in the absence of dust entraiment. Figure 2.2 also shows the profile of root mean square streamwise velocity fluctuation which tends to be roughly 10% of the free stream velocity (Schlichting, 1968). As a rule of thumb, the peak of the root mean square transversal velocity fluctuation is roughly 5% of the free stream velocity, and occurs at a greater distance from the wall. The latter fluctuation component is a mechanism aiding migration of entrained particles away from the layer.

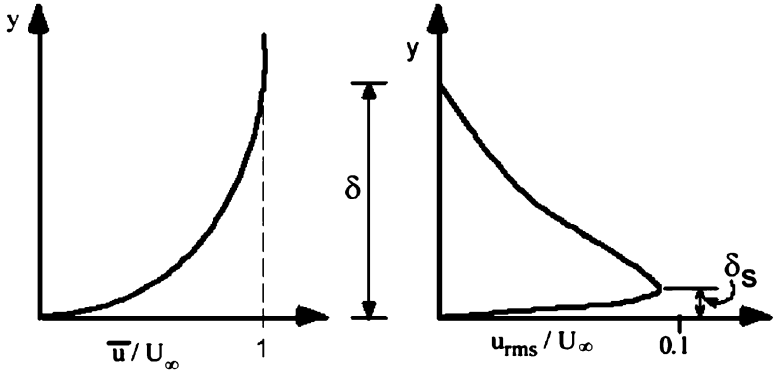

Fig. 2.2 Typical streamwise velocity profiles inside the boundary layer: mean velocity (left), root mean square of the fluctuating velocity (right)

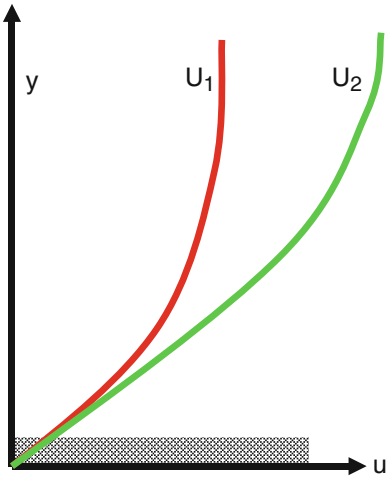

Fig. 2.3 Typical streamwise mean velocity profiles inside the boundary layer for two different friction coefficients and free stream velocities

The foregoing discussion suggests that aerodynamic forces acting on particles in a dust layer increase with increasing free-stream velocity. In early studies, the entrainment threshold or the entrainment amount had been correlated to the free stream velocity. In reality, small dust particles of interest here fall deep into the boundary layer as shown in Fig. 2.3. As a result, the layer is affected by the velocity gradient (or the boundary layer thickness) more so than the free stream velocity. That is why, in modern studies, the entrainment threshold or the entrainment amount had been correlated to the velocity gradient (γ), the shear stress (τw),

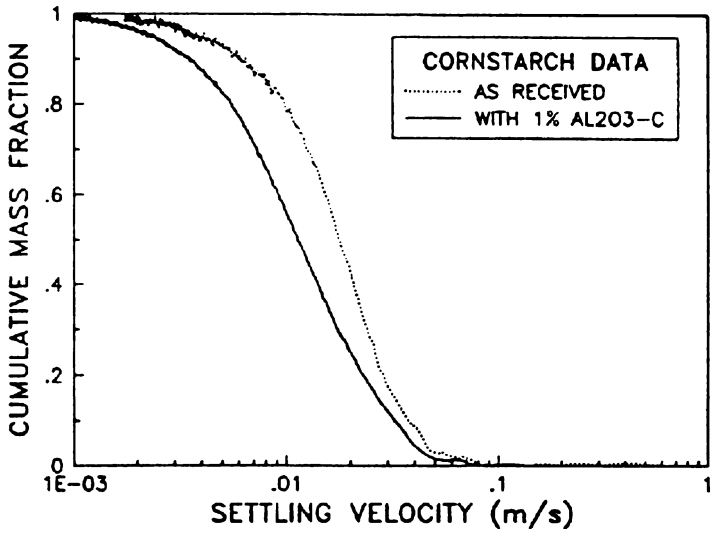

Fig. 2.4 Settling velocity of cornstarch with or without flowability agent Al2O3-C

or the friction velocity (interchangeably termed u_*, U_f or u_τ). By definition, these three parameters are uniquely related to each other through:

$$\tau_w = \mu\gamma = \rho u_\tau^2 \tag{2.10}$$

It is also conventional to define a friction coefficient, C_{fo} relating the friction velocity (u_τ) to the free stream velocity (U_e) through:

$$\tau_w = C_{fo}\mathbf{1}/\mathbf{2}\rho U_e^2 \tag{2.11}$$

Where the subscript o designates the friction coefficient in the absence of dust entrainment.

The presence of a dust cloud in suspension complicates the turbulence field. The dispersed phase affects both the mean and fluctuating components of the flow field. A review of this subject can be found in Faeth (1987). As will be discussed later, the entrainment process also effects the boundary layer properties.

The scope of this discussion thus far is limited to spherical particles. Most real particles, however, are of non-spherical shape, which introduces another source of uncertainty to the analyses. Depending on the profiles they present, non-spherical particles can generate significant lift forces. Correction factors to the drag coefficient of some special cases of non-spherical particles have been developed; a review of this topic was given in Carmichael (1984).

Ural (1989) developed a test method to measure the settling velocity distribution of dust samples. Typical data is shown in Fig. 2.4 for corn starch with or without electrical conductivity additive.

2.3 Characterization of the forces Conserving the layer

For horizontal layers, gravity holds the particles in place. The weight of a spherical particle can be calculated from:

$$W = 1/6\pi\boldsymbol{\rho}_p D^3 \tag{2.12}$$

Other forces include adhesion/cohesion, chemical bonds and mechanical interlocking (as in long fibers). Frequently cited classical reviews of this topic include Corn (1966), and Zimon (1982).

Various methods have been used to measure the adhesive forces. When the adhesive force is smaller than the particle weight, the adhesive force can be determined from the tilting angle of the surface at the time particles fall. Similarly, in the pendulum method a particle is attached to a fiber and hangs freely. A surface (or another particle to measure cohesion) is placed in contact with the suspended particle, and then pulled away in a direction perpendicular to the suspending fiber, until the particle detaches from the surface. The adhesion force is calculated from the slope of the fiber at the moment of detachment. For larger adhesive forces, microbalance techniques are used where the particle is attached to a micro-force measurement system (which can be an electronic balance, a spring, or a cantilevered beam). Both the pendulum and microbalance techniques are limited to relatively large particle sizes because small particles are very difficult to attach to the suspending fibers.

Adhesion forces of smaller particles are measured more conveniently using the centrifuge and the vibration methods. Both methods are capable of measuring adhesive forces up to 10^6 times the particle weight.

The studies of adhesion have revealed that for particles of approximately identical size, under identical conditions, the forces of adhesion will not all be the same; in fact, they may span several orders of magnitude. Recognizing this highly statistical nature of the adhesion forces, an adhesion number is defined as the fraction of particles removed when subjected to a given force. The statistical nature of the adhesion/cohesion forces is also responsible for the kinetic behavior of the entrainment flux. In other words, under steady-state exposure to a turbulent aerodynamic disturbance, entrainment flux changes with time.

From the theoretical standpoint, a number of mechanisms are recognized as playing a role in adhesion/cohesion of powders in air. Molecules making up the particles possess attractive force fields (Van der Waals) around them, which in effect, hold them together. The force fields of the molecules near the particle boundary are not neutralized, thus providing an adhesion force. The force fields of the individual molecules have been integrated over the particle volume to obtain the net attraction force between two spherical particles of diameter D1 and D2. The result, called the Van der Waals Force, is

$$F_m \alpha \frac{1}{Z_0^2} \cdot \frac{D_1\, D_2}{D_1 + D_2} \tag{2.13}$$

where, Z_0, the separation distance between the particles, is a major source of uncertainty[2] in determining the molecular forces. The attraction force between a spherical particle (of Diameter D) and a flat plate can be obtained by allowing D2 to go to infinity:

$$F_m \alpha \frac{1}{Z_0^2} \cdot D \tag{2.14}$$

The constant of proportionality in these equations varies by orders of magnitude for different materials, and is generally higher for softer material (e.g., plastics versus abrasives) that can deform and provide an increased contact area. Presence of flaws and trace impurities are also known to affect the Van der Waals forces. The variation of. the Van der Waals forces under identical conditions is blamed (Zimon, 1982) on the "energetic inhomogeneity" of solid surfaces, as well as the microsurface roughness.

The second well studied mechanism of adhesion is due to capillary condensation (also known as formation of liquid bridges). The water vapor (or solvent vapors) may condense in the vicinity of contact of two bodies, even when the vapor phase is below saturation, because a negative curvature exists in the contact area, and the equilibrium vapor pressure is a function of surface tension and curvature. The condensed liquid forms a film that draws the two bodies together because of surface tension and capillary pressure. The diameter of the liquid bridge is usually small compared to the particle diameter so that the adhesive force due to capillary pressure is negligible compared to that for surface tension. For completely wetting smooth surfaces, the adhesive force between a spherical particle and a flat surface is given by

$$\mathrm{F_L} = 2\pi\boldsymbol{\sigma}\mathrm{D} \tag{2.15}$$

where $\boldsymbol{\sigma}$ is the surface tension of liquid in contact with air, and D is the particle diameter. The adhesive force between two spheres of the same diameter is one half of the value calculated from this equation. Experimental evidence shows that the capillary condensation of water begins to occur at relative humidity levels above 70 percent.

There are two types of electrostatic forces that may play a role in particle adhesion. The first type arises from the contact potential, developed between the surfaces of two different materials. Ranade (1987) states that this type of force increases linearly with particle size, while Zimon (1982) recommends a two—thirds power dependence on particle size. The second type of electrostatic force is due to electric charges on the particles or the plate and is called the Coulomb force.

[2] The separation distance is usually not a directly measurable quantity for dusts, and assumptions for its value range typically from 0.4 to 1.0 nm.

For a spherical particle possessing an electrical charge, Q, resting on a flat uncharged surface, the Coulomb force is given by

$$F_c = \frac{Q^2}{6(Z_0 + D)^2} \tag{2.16}$$

where is Z_0 the separation distance, and D is the particle diameter. This equation exhibits the reduction in Coulomb force with increasing particle size if the particle charge were to be constant. However, particle charge may also depend on the particle size. Dust particles dispersed by air demonstrate charges increasing slightly less rapidly than the square of the diameter, so that the Coulomb forces may also increase with the square of the diameter. It should be noted that the charge on particles contacting a surface will change with time due to electrical leakage. Another important feature of the Coulomb forces that is different from the other types of adhesion forces is that they decay relatively slowly with distance, and these forces may play a role even after the initial dislodgement (e.g., Owen (1969)).

Other types of adhesion mechanisms include magnetism, acid—base interactions (Ranade, 1987), capillary pressure in pore spaces filled with liquid, highly viscous binding agents, and crystal bridges (Rumpf, 1977).

It is clear from the foregoing discussion that the adhesion theory is far from being a predictive tool, at this time. The most important conclusion, however, is that adhesive forces are typically proportional to the particle size. Since the particle weight is proportional to the cube of the particle size, the forces holding the particle down in a layer is expected to be dominated by the adhesive force for the small particles, while it is controlled by the particle weight for large particles. This fact explains the reason why larger particles produce more repeatable and more predictable results.

For small particles, experimental studies sometimes produced contradictory results. Direct as well as inverse dependence of adhesive force on particle diameter (or sometimes even complete independence) has been reported. Zimon (1982) attributed those contradictions to the statistical nature of adhesive forces. The curves of adhesion number versus adhesion force for different sizes of the same material are usually not parallel to each other and curiously tend to cross each other. Depending on the location of the adhesion number taken to characterize adhesion with respect to cross-over part of the curves, contradictory results will be obtained.

2.4 Fundamental Studies of Particle Removal from Surfaces

This continues to be an active research area and a large body of experimental and theoretical work has already been published. A review of the topic can be found in Ziskind et al (1995) and Gradon (2009). Experiments indicate that adhesion forces as well as the aerodynamic forces exhibit a stochastic distribution. Coherent structures in the airflow play a significant role on the threshold entrainment

conditions as well as entrainment rates. As a result, entrainment rate is not constant under specified conditions, but varies as a function of time.

Other experimental variables include underlying surface material, surface roughness, particle moisture, and the presence of an electrical field. In general, existing theoretical models are incapable of predicting the experimental data.

Some of the recent noteworthy publications include Ibrahim et al (2008), Jiang et al (2008), Merrison et al (2007), Grzybowski and Gradon (2005 and 2007), Masuda et al (1994), Gotoh and Masuda (1998), Hayden et al (2003), Rasmussen et al (2009), Roney and White (2006), Brateen et al (1990), Friess and Yadigaroglu (2002).

2.5 Applied Research on Aerodynamic Entrainment Threshold

At this point, it should be clear that first principle modeling of aerodynamic entrainment threshold or entrainment flux does not promise much success due to large gaps in current capabilities to predict the aerodynamic forces as well as the forces conserving the layer. For that reason, many studies have been carried out in wind tunnels or in open atmosphere and correlations have been proposed. While these correlations might be extrapolated to similar flow conditions and dusts, the major difficulty with this approach is that the results can not be generalized to all dusts.

Early work of Bagnold (1941) is still the most cited reference of the field. Bagnold studied the conditions leading to the saltation phenomenon by spreading a thick layer of sand on the bottom of a 30 × 30 cm cross-section wind tunnel using mean air velocities up to 10 m/s. The sand particles were typically 100 microns or more in size so that adhesive forces were negligible compared to particle weight. Bagnold determined that in order to initiate grain movement, the condition:

$$\boldsymbol{\tau}_w > 0.01 \boldsymbol{\rho}_p g D \tag{2.17}$$

must be satisfied. In this equation, $\boldsymbol{\tau}_w$ denotes the wall shear stress[3], whereas $\boldsymbol{\rho}$p, D, and g represent the particle density and diameter and the gravitational acceleration, respectively. Bagnold also discovered that the saltation, once initiated artificially at shear stresses below the value of initiation value, can sustain itself so long as:

$$\boldsymbol{\tau}_w > 0.0064 \boldsymbol{\rho}_p g D \tag{2.18}$$

[3] In the literature, three parameters are used commonly to characterize the flow conditions near the wall: wall shear stress, $\boldsymbol{\tau}_w$, velocity gradient, $\boldsymbol{\gamma}$; and friction velocity, u_τ (or u*). These three parameters are uniquely related to each other through the following relationship: $\boldsymbol{\tau}_w = \boldsymbol{\mu}\,\boldsymbol{\gamma} = \boldsymbol{\rho}\, u_\tau^2 = \boldsymbol{\rho}\, u_*^2$

is satisfied. These equations are often referred to as the static and dynamic thresholds of saltation, respectively. The reason for the dynamic threshold being lower than the static threshold was explained by the ejection of new particles from the layer upon impact of saltating particles. Bagnold observed that the saltating particles leave the surface vertically at a velocity comparable to the friction velocity of the boundary layer. As discussed earlier, the aerodynamic lift acting on the particle is too small to explain this behavior. Therefore, the particle ejection is believed to be due to impact of either rolling or saltating particles. On this basis, however, it is hard to rationalize the observation that a factor of from two to twenty-five more mass is being conveyed by jumping than by rolling for various sand and soils (Fuchs (1964)).

Bagnold's data obtained for sand particles typically larger than 100 um have shown that smaller particles are moved more easily than larger particles. Numerous experiments performed later with smaller particles have shown that this trend is reversed for fine particles, so that the plots of threshold shear stress as a function of particle size have a minimum. The particle size for minimum threshold shear stress (i.e., for optimum dispersion) has been found to vary with the type of powder tested and may also be dependent on the details of the experimental conditions. For example, Zimon (1982) quotes optimal particle sizes of 15-20 um for sylvite dust and 100—150 um for corrundum particles laying on a steel wall. Similarly, Allen (1970) quotes an optimal diameter of about 100 um for quartz density sand. The increase of aerodynamic wall shear stress required to move smaller particles is widely believed to be due to adhesive forces. The adhesive forces are typically proportional to the particle size, whereas the gravitational force is proportional to the third power of the particle size, so that the former should dominate the latter for sufficiently small particles. The aerodynamic forces, reviewed earlier in this section, are typically proportional to the square of the particle diameter. Therefore, apparent contradiction in large versus small particle trends are explainable through force-balance theories.

Figure 2.5 shows the force-balance theory predictions for spherical sand particles ($\rho p = 2500$ kg/m3) in air by Phillips 1980. According to his theory, for large particles, line DE represents the condition

$$\text{Aerodynamic drag force} = \text{Particle weight}$$

which resulted in $\boldsymbol{\tau}_w \boldsymbol{\alpha}$ D.

For small particles, line XY represents the condition:

$$\text{Aerodynamic lift} = \text{Particle adhesion force}$$

which resulted in $\boldsymbol{\tau}_w \boldsymbol{\alpha}\ D^{-4/3}$.

For intermediate size particles, Phillips postulated

$$\text{Aerodynamic lift} = \text{Particle weight}$$

which resulted in threshold shear stress being independent of particle size.

Numerous studies describing force-balance models and resulting threshold shear stress (or equivalently threshold friction velocity as defined in footnote 5) curves have been published.

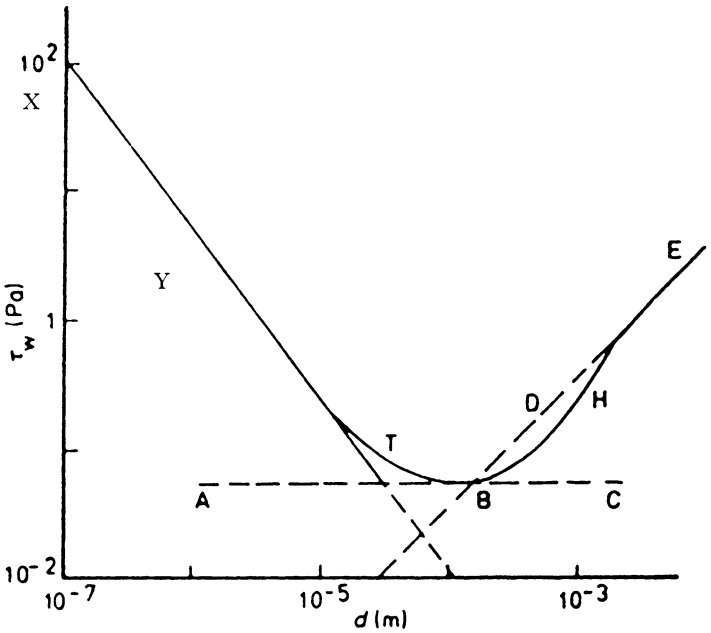

Fig. 2.5 Prediction of a force-balance theory for spherical sand particles in air

Figure 2.6 shows such a curve for threshold shear velocity versus particle size derived for wind erosion of sand (Greely and Iverson, 1985). Also superimposed on this figure are lines for constant value of the terminal velocity to friction velocity ratio delineating different modes of entrained particle motion.

For cohesive dusts, the threshold shear stress (or friction velocity) for particle movement is recognized to depend strongly on the conditions the deposit has been subjected to since its formation. For example, for erosion of desert soils, Gilette (1978) recommended actual field measurements using a portable wind tunnel with an open-floored test section.

A review of the Soviet activity on aerodynamic removal of powders from solid surfaces is given in Chapter 10 of Zimon (1982). The various experiments described by Zimon include removal of dust particles by air flow inside long ducts, detachment by a developing flow over a flat plate at various angles of attack, as well as detachment of particles from cylindrical surfaces by external air flow. Zimon at times has omitted some of the essential information in his review so that original papers may have to be referred to before using the data. In an interesting experiment described by Zimon (1982), spherical glass particles of varying diameter were placed on a steel plate with a Class IV surface finish[4] and were subjected to

[4] This is a Russian designation of surface roughness which corresponds to asperity height of 40 microns (1600 micro-inch).

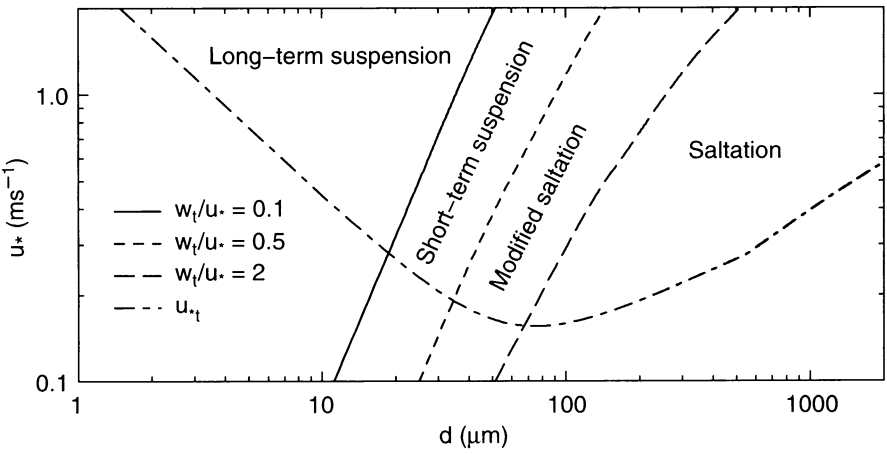

Fig. 2.6 Threshold shear velocity and suspension modes for wind erosion of sand

a 6.2 m/s free stream velocity. The shear stress on a flat plate decreases with increasing distance from the leading edge; therefore, close to the leading edge, all the particles are removed, but away from the leading edge none of the particles are removed. Zimon (1982) used the observed distances for complete removal and no removal to estimate the aerodynamic force required to remove the particles. There are several drawbacks associated with this type of experiment:

(1) the fact that the boundary layer equations are singular near the leading edge introduces some uncertainty in calculated flow conditions in this area;
(2) sufficiently away from the leading edge, the boundary layer may display transition to turbulence which introduces additional uncertainty to the calculated wall shear stresses;
(3) the removed particles transported downstream towards the undisturbed area may have an effect on the critical distance measured for no particle removal; and
(4) the shear stress, in the laminar flow regime, is inversely proportional to the square root of the distance from the leading edge, so that a relatively long plate must be used to observe both distances for complete and no particle removal in a single experiment.

Figure 2.7 shows the "lift-off" apparatus developed by Ural (1989) to determine the aerodynamic forces required to remove a dust deposit. Air moves radially inward between the two disks accelerating towards the center due to the reduction in the effective cross-sectional area. In addition to radial variation, the local air velocity is controlled by means of changing the gap between the plates and by adjusting the total airflow rate through the system. Calibration charts were developed to look up shear stress corresponding to a given radius (of the particle free circle created by the flow) at a given gap and pressure drop. Figure 2.8 shows a typical dust removal pattern which would be considered acceptable for the test method.

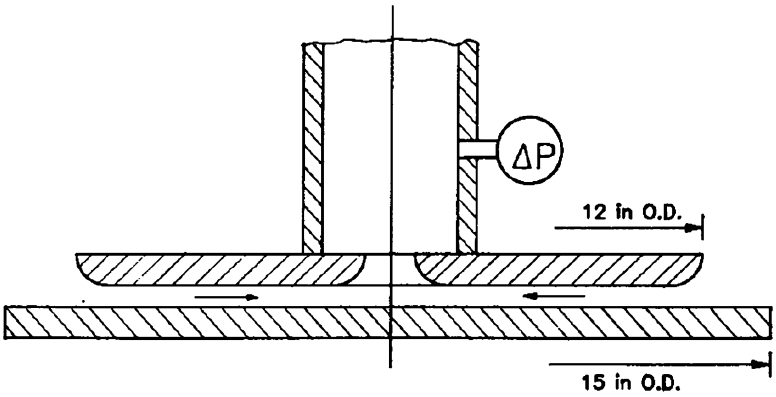

Fig. 2.7 Lift-off apparatus to determine the aerodynamic forces required to remove a dust deposit

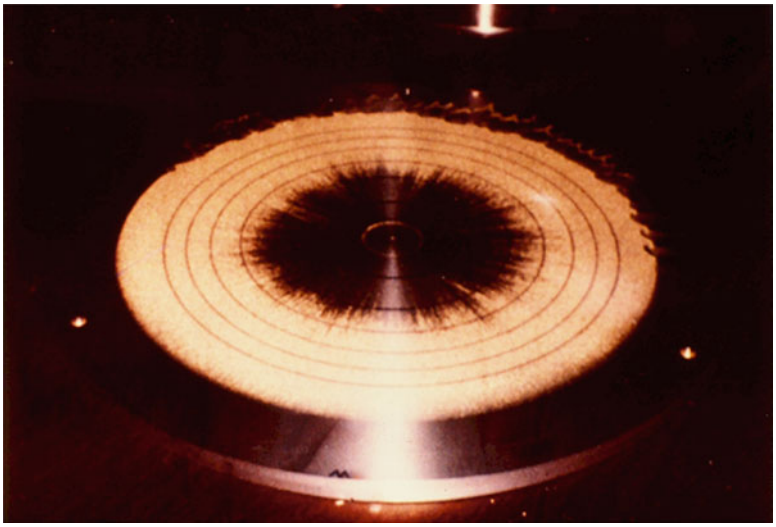

Fig. 2.8 Dust removal pattern in the lift-off apparatus

Recently, Kalman et al (2005) proposed a general correlation based on particle Reynolds number, Rep, and the Archimedes number, Ar. The correlation, in the form of three piecewise continuous equations appear to correlate bulk velocity for pick up threshold, U_{pu}, in gases as well as in liquids:

$$\text{Zone I} \quad \mathrm{Re}_p^* = 5\mathrm{Ar}^{3/7} \tag{2.19}$$

$$\text{Zone II} \quad \mathrm{Re}_p^* = 16.7 \tag{2.20}$$

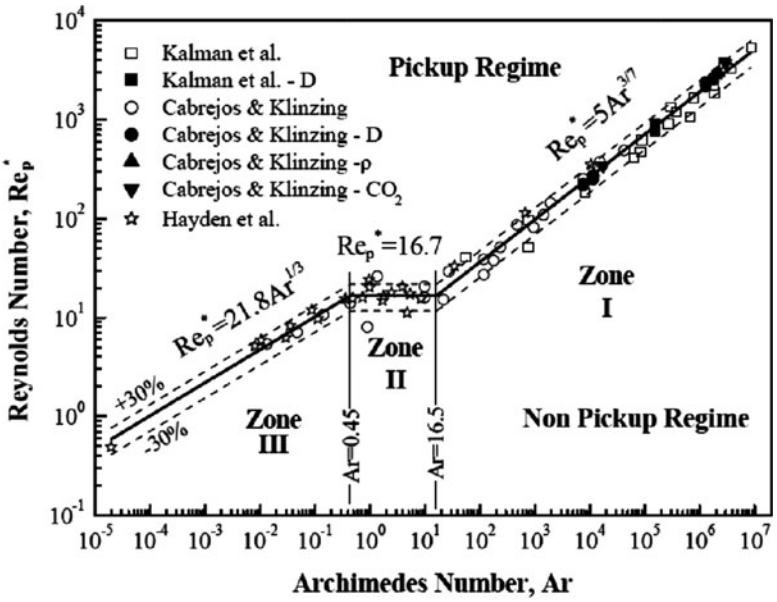

Fig. 2.9 Comparison of Kalman et al (2005) correlation with data

$$\text{Zone III} \quad \mathrm{Re}_\mathrm{p}^* = 21.8\mathrm{Ar}^{*1/3} \tag{2.21}$$

Where:

$$\mathrm{Re}_\mathrm{p}^* = \frac{\rho \cdot U_{pu} \cdot d}{\mu \cdot \left(1.4 - 0.8 \cdot e^{-\dfrac{D/D_{50}}{1.5}}\right)} \tag{2.22}$$

$$Ar = \frac{g \cdot \rho \cdot \left(\rho_p - \rho\right) \cdot d^3}{\mu^2} \tag{2.23}$$

d: particle diameter
D: pipe diameter
μ: dynamic viscosity
g: gravitational acceleration
ρ: fluid density
ρp: particle density
Ar* = 0.03 e3.5**ϕ** Ar, modified Archimedes number
ϕ: particle sphericity

A correction factor for non-spherical, relatively large particles was also provided. Figure 2.9 shows the goodness of how their correlations match the gas pick-up data,

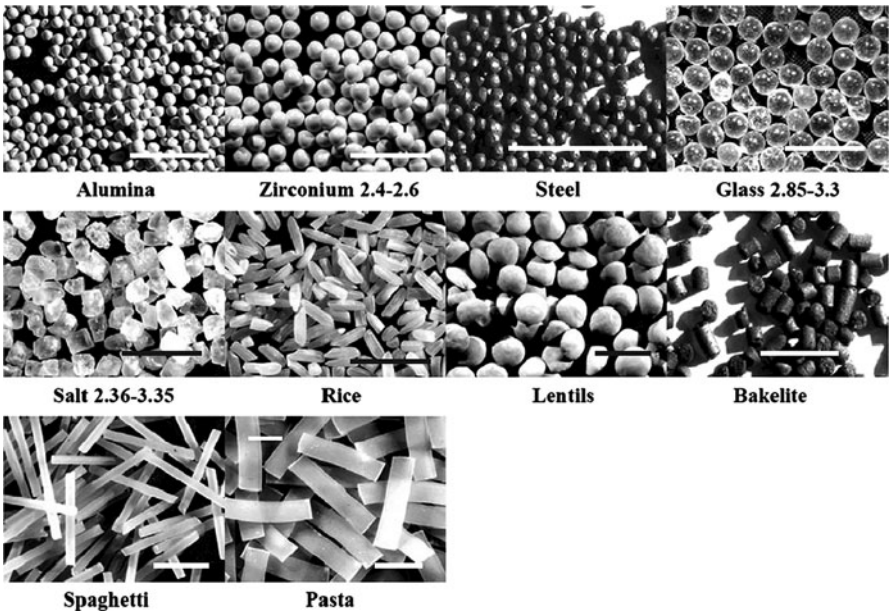

Fig. 2.10 Shapes of non-spherical particles

and Fig. 2.10 shows types of particles used to validate the non-spherical particle correction factor. Fig. 2.11 shows the threshold (pickup) velocities calculated for spherical glass particles.

2.6 Applied Research on Aerodynamic Entrainment Mass Flux

The measurement of this parameter is significantly more difficult than the entrainment threshold.

Measured values of dust emission by wind erosion typically range from 10^{-7} to 0.1 g/m2-s, because of the relatively low velocities experienced in natural winds. Gillette (1977) carried out indirect measurements of entrainment mass flux for nine different soils as a function of friction velocity. The large degree of scatter in the data did not permit development of a definitive correlation. Data seem to support the power relationship between the mass flux $\mathbf{\Phi}$ and shear velocity u_* through

$$\mathbf{\Phi \alpha u_*^n} \tag{2.24}$$

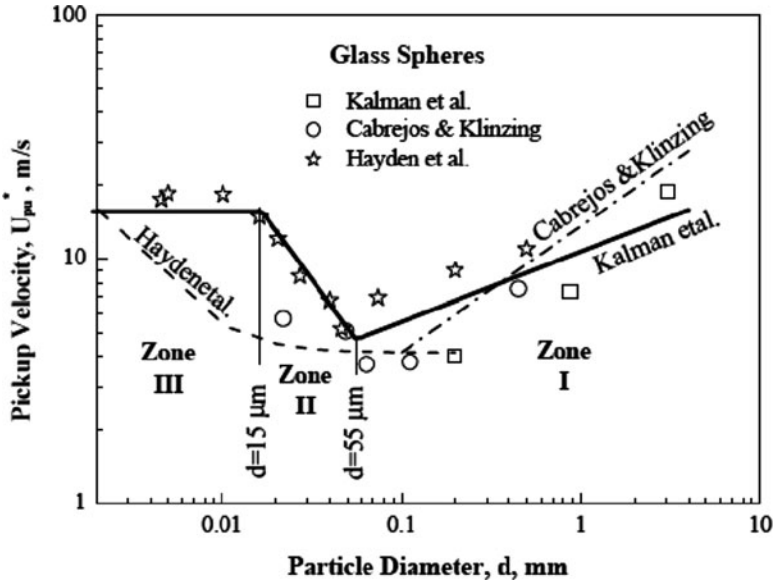

Fig. 2.11 Comparison of Kalman et al (2005) correlation with data for glass spheres and other correlations

Where exponent n could range from 3 to 5. Later, Gillette and Passi (1988) suggested a relationship, which takes threshold entrainment velocity, $\mathbf{u_{*t}}$ into account:

$$\Phi = \alpha_g \mathbf{u}_*^4 [\mathbf{1} - \mathbf{u}_{*t}/\mathbf{u}_*] \tag{2.25}$$

where $\boldsymbol{\alpha_g}$ is a dimensional coefficient. It should be noted that, at high free stream velocities, boundary layer is affected by the large entrainment mass flux and the exponent n could be as low as unity.

Hartenbaum (1971) performed a limited number of steady state entrainment tests in a wind tunnel which had a test section 40″ high and 18″ wide. Free stream velocities ranged from 34 to 115 m/s. A particulate bed approximately 4″ deep at the start of each test was composed of AFS 50-70 Ottawa silica testing sand which had a mean particle diameter of 250 um. The entrainment rate was correlated to the free stream velocity U with the following equation:

$$\Phi(\mathbf{1b/ft2} - \mathbf{s}) = \mathbf{0.366\ 10^{-2}} [\mathbf{U(ft/s)}]^{\mathbf{5/4}} \tag{2.26}$$

Hartenbaum also took time to characterize the boundary layer at the test section and fitted a correlation to the shear velocity:

$$\Phi(\mathbf{1b/ft2} - \mathbf{s}) = \mathbf{0.86\ 10^{-3}} [\mathbf{U_*(ft/s)}]^{\mathbf{5/4}} \mathbf{-0.01} \tag{2.27}$$

Later, upon request from the US Bureau of Mines, Rosenblatt recast the Hartenbaum's free stream velocity equation to include air density effect in an ad hoc fashion. He also included an ad hoc threshold free stream velocity effect to make the entrainment flux nil at 420 cm/s for mine applications. The resulting equation:

$$\dot{m}'' = \rho \cdot U \cdot \left[0.0021 \cdot U^{0.25} - \frac{4}{U}\right] \tag{2.28}$$

is still being used by NIOSH for mine research purposes (Edwards and Ford, 1988). Bureau of Mines measurements (Singer, Harris and Grumer, 1976) indicate that gas-explosion induced air flow threshold velocities are in the range of 5 to 30 m/s for coal dust. It is noteworthy to point out that both Hartenbaum and Bureau of Mines correlations, mass flux is proportional to the 1.25 power of the free stream velocity.

Batt et al. (1995) and Batt et al (1999) reported extensive entrainment data for high-speed air flow velocities, typically ranging from 100 to 300 ft/s. They developed the following correlation:

$$\dot{m}'' = (0.3 \pm 0.1)\frac{\rho_e \cdot U_f \cdot M_e^{0.5}}{\alpha/\alpha_{WMSR}} \tag{2.29}$$

where:

m'': entrained mass flux
$\boldsymbol{\rho}_e$: free stream air density
U_f: friction velocity
M_e: free stream flow Mach number
$\boldsymbol{\alpha}$: angle of repose of soil
$\boldsymbol{\alpha}_{WMSR}$: angle of repose for soil at the White Sands Missile Range

This equation appears to correlate well the entrainment rate of Ottawa Sand and White Sands Missile Range soil, over a wide range of parameters tested, and predicts mass flux to be proportional to the 1.5 power of the free stream velocity. Batt et al (1995) point out that the larger exponent of 3, proposed originally by Bagnold in 1941, may more appropriate for wind erosion where the free stream velocity is typically below 20 m/s.

The Batt equation above expresses the mass flux as a function of the friction velocity, U_f. For the ease of use, it may be preferable to recast equation on the free stream velocity, even at a cost of precision loss. Since the dust entrainment occurs deep in the boundary layer, friction velocity rather than the free stream velocity is the more appropriate parameter to correlate the entrainment rate. On the other hand, most users of the NFPA standards are not anticipated to be versatile in using aerodynamics concepts encompassing the friction velocity. Therefore, an additional simplification is introduced by translating the selected entrainment rate correlation

to free stream velocity. The original (2.29) is further modified here for low flow velocities so that entrainment rate tends to zero at the threshold velocity. Thus, the new equation proposed in this project is:

$$\dot{m}'' = (0.002) \cdot \rho_e \cdot U_e \left[U_e^{1/2} - \frac{U_t^2}{U_e^{3/2}} \right] \tag{2.30}$$

Where, U_e and U_t respectively represent the free stream velocity and the threshold (pickup) velocity. Equation (2.30), which constitutes the basis of our new strawman method described in the next chapter, is an improved version of the NIOSH equation (2.28), and includes an ad hoc correction for the appropriate threshold velocity. The coefficient 0.002 of (2.30) was selected to envelope the Batt et al data.

Zydak and Klemens (2007) studied the entrainment rates of dust deposits by airflow. Tests were conducted in a shock tube / wind tunnel with internal cross section 72 mm by 112 mm. Dust layer dust thickness tested were 0.1 mm, 0.4 mm or 0.8 mm. The following dimensional correlation was proposed by these authors:

$$\mathbf{\Phi} = 0.004 h_l^{0.216}\ U^{1.743}\ D^{-0.054}\ \boldsymbol{\rho}_p^{-0.159}\ Ap^{0.957} \tag{2.31}$$

Where:

Φ: entrained mass flux in kg/m2-s
h_l: layer thickness in mm
U: flow velocity above the layer in m/s
D: characteristic particle size um
$\boldsymbol{\rho}_p$: particle density in kg/m3, and
Ap: is a dimensional empirical constant.

This is in fact the dust entrainment correlation built into the current version of the DESC code. Equation 2.31 assumes that the entrainment mass flux is proportional to the 1.75 power of the free stream velocity.

The authors selected the following input parameters when developing their correlation:

Coal dust	1.2		1340
Potato starch	0.745	75	1469
Potato starch	0.7	35	1527
Silicon dust	1.037		2341

Shock tubes have been recognized as a valuable tool in studying aerodynamic dust lift—off because they provide a well defined flow environment. They also have a direct application in characterizing the dust lift-off by blast waves emanating from conventional or thermonuclear explosions. Some examples of this type of experiment performed with non- cohesive dust are given by Gerrard (1963), Fletcher (1976),

Boiko et al (1984), and the references therein. In interpreting shock tube data, one must be careful about the effect of streamwise compression of dust layer across the shock wave. This effect often causes a significant lateral dust ejection velocity and throws the particles beyond the viscous boundary layer.

Fletcher (1976) has subjected layers of treated (free flowing) limestone dust, typically 14 um in size, to Mach 1.15 to 1.3 incident shock waves. The convective flow velocities under these conditions vary between 80 and 150 m/s. The dust cloud shapes measured from photographs were shown to fit the ballistic trajectories of individual particles having an initial vertical velocity of about 14.5 m/s. Boiko et al (1984) have repeated Fletcher's experiments with a much stronger shock (Mach 2.6 corresponding to a convective velocity of 628 m/s). They report vertical ejection velocities of 40 m/s for 200 um glass particles ($\boldsymbol{\rho}_p = 1200$ Kg/m3), and 17 m/s for 200 um bronze particles ($\boldsymbol{\rho}_p = 8700$ Kg/m3).

The small cohesive particles may be lifted from the surface in the form of aggregates. The breakdown of these aggregates in a turbulent flow field is of importance in determining the extent of the dispersion. Singer et al (1976) noted mine dust deposits that have been wetted or have undergone a wetting-drying cycle may constitute a greater explosion hazard than untreated dusts owing to selective lifting of relatively large briquetted fragments which then dispersed in the air stream.

The theoretical progress in the field has been at a rather slow pace. A good physical description of the various phenomena encountered in the pneumatic transport of non-cohesive powders is given by Owen (1969).

Corn and Stein (1965) used the calculated particle drag force to interpret their aerodynamic dust entrainment threshold data. The drag force was calculated using the spherical particle drag coefficient, and the boundary layer velocity at one particle radius distance from the wall. For less than 53 um diameter glass beads deposited on glass slide, these authors report that at removal efficiencies exceeding 75%, the calculated air drag was Within a factor of 2.5 of the adhesion force measured using the ultracentrifuge method. At lower removal efficiencies, the two forces differed by as much as a factor of 10. Corn and Stein also report that for the turbulent boundary layers employed in their experiments, the dust removal efficiency is somewhat dependent on the test duration. Later, Zimon (1982) repeated these experiments using 20 and 35 um loess[5] particles and reported good agreement with the centrifuge method. The formulas used by Corn and Stein are at best rough estimates of the drag force (parallel to the surface) exerted by air as it is calculated from the undisturbed velocity in the boundary layer at the level of particle center. As was stated earlier, the actual drag force for creeping flow was 70 percent higher than that calculated by the Corn and Stein method. Furthermore, in turbulent flow, some form of a peak force (rather than mean) should be responsible for particle dislodgement.

[5] Loess is an unstratified, usually buff to yellowish brown, loamy deposit found in North America, Europe, and Asia and is believed to be chiefly deposited by the wind.

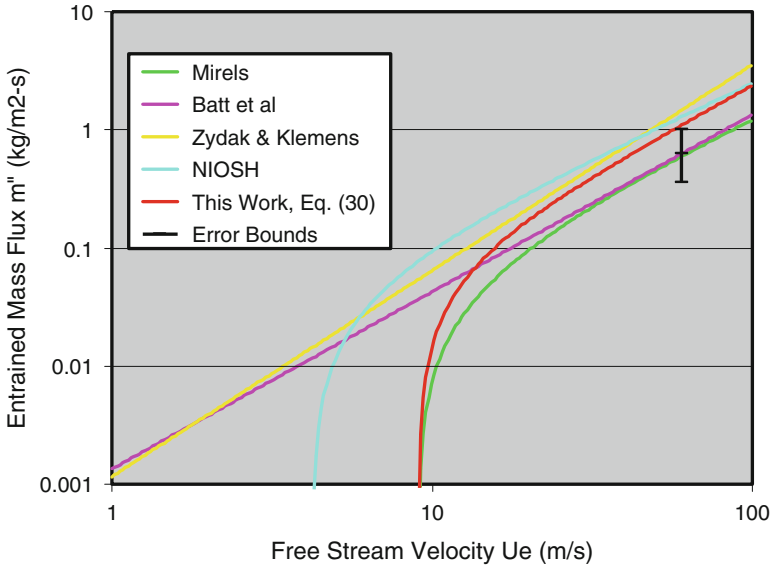

Fig. 2.12 Comparison of the predictions from various entrainment mass flux equations for 53 micron coal dust

Another interesting hypothesis advanced in Zimon's book was that the maximum diameter of the adherent particles remaining on a surface after being exposed to a turbulent boundary layer is equal to the thickness of the laminar sublayer. Zimon suggests the use of this hypothesis as a means to determine the laminar sublayer thickness. This hypothesis, although demonstrated with some experiments, is not completely substantiated.

The model of saltation phenomena given by Owen (1964) avoids these fundamental questions on particle removal using two key phenomenological hypothesis: (1) the effect of the moving grains on the fluid outside the saltation region is similar to that of solid roughness of height comparable with the depth of the saltation layer, and (2) the concentration of particles within the saltation layer is maintained to keep the wall shear stress at the dynamic threshold of Bagnold, given in (2.18). These two assumptions are validated by the agreement between the measured and predicted quantities. Owen (1964) also speculated that the particles would enter into suspension when the wall shear stress is of the same order of magnitude as $\boldsymbol{\rho}_p gD$.

Recently, Mirels (1984) has used Owen's second hypothesis to calculate the dust erosion rates in developing turbulent boundary layers over a flat plate and behind a shock wave. Treating the effect of dust entrainment on the flow with his previous transpiration model, Mirels reported agreement Hartenbaum's high entrainment rate with data within a factor of two. It is remarkable, if not fortuitous, that Mirel's simple conceptual model predicted the experimental velocity exponent very well.

Figure 2.12 compares the predictions of the several entrainment mass flux equations described in this section. Calculations were made for 53 micron coal

dust particles with a particle density of 1.34 g/cm3. Air density is taken to be 1.2 g/3. Kalman et al (2005) correlation results in a threshold (pick-up) velocity of 9 m/s for the onset of entrainment. The critical shear stress needed for the Mirels model was estimated to be 0.15 Pa from the threshold velocity, (2.10) and (11) using a friction coefficient of 0.003. The layer thickness needed for the Zydak and Klemens equation was assumed to be 1/32″.

All equations seem to agree with each other within a factor of three for the high speed flows. The disparity for low speeds were not unexpected since the NIOSH equation was forced to predict zero entrainment at 4.2 m/s, whereas Batt et al, and Zydak and Klemens correlation tend to no entrainment only when the free stream velocity approaches zero.

2.7 Secondary Explosion Propagation Tests

In these experiments combustible dust deposited on the floor of a gallery is dispersed and ignited by a primary explosion at the beginning of the gallery. Measurements typically include pressure development, apparent flame speeds, and gas velocities. Examples of these types of experiments can be found in Tamanini (1983), Richmond and Liebman (1974), and Michelis et al (1987). These experiments are quite costly, and therefore have been performed using very few types of dusts (mostly coal dust, and some cornstarch). Since a number of phenomena play crucial roles in sequence in these experiments, the results are often not repeatable. In order to improve the repeatability problems, the tests are designed so that the secondary explosion is overdriven by a strong primary explosion.

Similar tests have been carried out at intermediate scale. Tamanini (1983) used a 6 m long model gallery with 0.3 m2 cross-section to study secondary explosions of cornstarch. Recently, Srinath et al (1987) tested a number of dusts in their 0.3 m I.D. 37 m long flame acceleration tube. The scaling of test results from intermediate scale to actual size galleries should be difficult, at best.

Investigations aimed at understanding the aerodynamic dust entrainment in mine galleries have been carried out at the U.S. Bureau of Mines, as an extension of the early British work (Dawes, 1952).

Singer et al (1969) measured the minimum air velocities required for dispersal of coal and rock dust deposited at the floor of a small wind tunnel test section (7.62 cm wide, 2.54 to 5.08 cm high). Tests have been carried out using monolayer dust deposits, as well as piles of dust. The effects of type of surface holding the dust, relative humidity of the dust pre- conditioning atmosphere, and the large-amplitude oscillations superimposed on the air stream on the threshold dust entrainment velocity were studied. The air flow rate was transient during the tests, with a reported rise time of 1 minute.

In the monolayer studies, the average air velocities required to remove 25, 50 and 75 percent of the particles (by microscopic number count) were determined.

The measured threshold velocities for 75% dust removal ranged from 20 to 130 m/s, increasing with decreasing particle size. The calculated wall shear stresses in this configuration range from 1 to 30 Pa. The measured threshold entrainment velocities for the three types of dust tested increased in the order: rock dust, anthracite, and Pittsburgh seam coal. The differences in the threshold velocities of these dusts diminished for particle sizes below 10 um. The rock dust was removed more easily from smooth Pittsburgh seam coal and glass surfaces than from smooth anthracite.

In tests with dust piles, the minimum air velocity required for complete removal of the dust pile was measured. Velocity measurements were taken upstream of the pile, at a distance from the tunnel floor equal to mid-height of the ridge. The types of dust removal observed included erosion, denudation, as well as removal of massive clumps and sliding of the entire ridge. The reported threshold velocities spanned the range from 5 to 23 m/s. It was found that the compaction of ridge significantly increases the threshold entrainment velocity, whereas the presence of vibrations either in the air flow or on the floor reduces it. The relative humidity of dust in the range of 35 to 90 percent was found to have no significant effect on the threshold velocity. Interestingly, for the dust piles tested, anthracite dust was easiest to be removed, while rock dust was the most difficult, an order different than observed for monolayers.

Singer et al (1972) have later attempted to relate the entrainment threshold of dust piles to the shear cell data believed to be some representation of the cohesive forces between the particles. First, they have defined a threshold Froude number:

$$Fr = \frac{\tau_w}{\sqrt{\rho_b g \tau_y H/2}}$$

where:

$\boldsymbol{\tau}_w$ aerodynamic wall shear stress;
$\boldsymbol{\tau}_y$ shear cell yield stress extrapolated to no load;
$\boldsymbol{\rho}_b$ bulk density of powder;
gravitational acceleration; and
height of the dust piles.

The denominator was stated to be the "geometric mean of the gravitational and cohesive forces," yet it lacks any physical significance. Singer et al (1972) found that for their limited number of data points, this Froude number remained relatively constant within the range 0.0077 to 0.038 for their dust ridges and beds. These authors also tried the ratio of the aerodynamic dynamic pressure at the mid-height of the pile to Ty and found it to cover the range between 0.22 and 0.75.

A limited number of threshold tests were repeated in a large scale (1.5 m high, and 2.4 m wide) wind tunnel, which indicated that the threshold velocities in the large scale wind tunnel is a factor of 1 to 3 smaller than those measured in the small wind tunnel. These authors have also made some entrainment rate measurements and presented their results as data correlations. These correlations must be used

with extreme caution beyond their intended range or for different dusts because they are not based on physical reasoning.

In a follow-up, work Singer et al (1976) have used actual explosion induced air flow, fraction of a second in duration, to study the dust dispersion phenomena. Most tests were carried out in a 0.61 m I.D. 49.7 m long explosion tunnel, while some tests were repeated in the full scale experimental mine gallery. The instantaneous threshold air velocities in these explosion tests were found to be in the same range as the earlier slow-rise threshold velocity tests described above. One of the important objectives of this study was to study the selective dispersion of coal dust over rock dust, which would decrease the inerting probability. It was found that the uniformly mixed beds always dispersed without separation, whereas in the case of coal dust layer deposited over a rock dust layer, only the coal dust is dispersed if the peak airflow velocity is in a range between the threshold velocities of the two dusts.

Hwang et al (1974) modeled the dispersion phenomena using the diffusion equation. The details of the entrainment were completely ignored and the entrainment rate, specified as a denudation rate, was left as input. This model also ignores the effects of gravity. There is also a great uncertainty in picking a diffusion coefficient which was stated to be between 0.2 to 362 cm2/s. These authors recommended the use of diffusion coefficients in the range 25 to 100 cm2/s as "best guess," which results in a factor of four variation in the calculated dust concentration.

The modeling effort at the University of Michigan was focused on the coupling of the dust lift-off with flame propagation. In this model, the one-dimensional flame propagation model of Chi and Perlee (1974) was mated with the entrainment rate model of Mirel (1984) described above. The agreement with the data given in Srinath et al (1987) was qualitative. The limitations of this approach arose from the fact that the mixing process and the effects of gravity were not included. More recently, Li et al (2005) examined the possibility of deflagration to detonation transition supported by layers of corn dust, cornstarch, Mira Gel starch, wheat dust, and wood flour. Flame speeds of up to 1300 m/s were observed, which the authors called quasi-detonations.

2.8 Computational Simulation of Aerodynamic Dust Entrainment Phenomena

Computational Fluid Dynamics (CFD) tools have also been used to predict the entrainment phenomena. Iimura et al (2009) studied the removal agglomerates by shear flow, using a modified discrete element method. Ilea et al, in University of Bergen developed an Eulerian-Lagrangian model and studied various aspects of dust entrainment behind a shock wave.

Dust Explosion Simulation Code (DESC) is a CFD models sometimes used to simulate secondary explosions. However, as was discussed above, these models rely on very crude correlations to represent the entrained mass flux. Hence, it is hoped that the CFD models too will benefit from this project.

2.9 Gaps in Available Information

This study revealed serious gaps in the available information.

Even though a large body of fundamental experimental and theoretical work has already been published, existing theoretical models are incapable of predicting the experimental data. This difficulty is inherent in the phenomena involved in dust entrainment, as experiments indicate that adhesion forces as well as the aerodynamic forces exhibit a stochastic distribution. Coherent structures in the airflow play a significant role on the threshold entrainment conditions as well as entrainment rates. As a result, entrainment rate is not constant under specified conditions, but varies as a function of time. Additionally, factors such as underlying surface material, surface roughness, particle moisture, and the presence of an electrical field also display significant effects.

Applied research focused on specific applications thus resulting in more encouraging predictive tools. There exist a significant number of publications, which can be distributed into clusters such as atmospheric erosion, pneumatic transport, fluidization, pharmaceutical delivery, atmospheric emission. Unfortunately, due to limitations in applicability, these studies are not directly useable for the present project.

There exist a limited number of experimental studies secondary explosions. However, scale, geometry and the parameters of these tests limit their generalization to the broad range of industrial applications.

http://www.springer.com/978-1-4614-3371-2

Towards Estimating Entrainment Fraction for Dust Layers

Ural, E.A.

2011, XVIII, 70 p. 28 illus., Softcover
ISBN: 978-1-4614-3371-2